An exploration on collapse mechanism of multi-jet flash-boiling sprays

Article *in* Applied Thermal Engineering · April 2018

DOI: 10.1016/j.applthermaleng.2018.01.102

8 authors, including:

Yanfei Li
Tsinghua University
44 PUBLICATIONS **126** CITATIONS
SEE PROFILE

Hengjie Guo
Tsinghua University
16 PUBLICATIONS **39** CITATIONS
SEE PROFILE

Shubo Fei
Tsinghua University
3 PUBLICATIONS **1** CITATION
SEE PROFILE

Xiao Ma
Northwestern Polytechnical University
79 PUBLICATIONS **601** CITATIONS
SEE PROFILE

Applied Thermal Engineering 134 (2018) 20–28

Contents lists available at ScienceDirect

Applied Thermal Engineering

journal homepage: www.elsevier.com/locate/apthermeng

Research Paper

An exploration on collapse mechanism of multi-jet flash-boiling sprays

Yanfei Li[a], Hengjie Guo[a], Shubo Fei[a], Xiao Ma[a], Zhou Zhang[a], Longfei Chen[b,*], Liuyang Feng[b], Zhi Wang[a]

[a] State Key Laboratory of Automotive Safety and Energy, Tsinghua University, Beijing 100084, China
[b] School of Energy and Power Engineering, Beihang University, Beijing 100191, China

HIGHLIGHTS

- Collapse of multi-jet flash-boiling sprays was caused by vapor condensation.
- Jet overlap was a necessary condition for collapse of flash-boiling sprays.
- Collapse under high P_{amb} was caused by low-pressure induced by high-speed jets.
- Rapid bubble bursting caused local static pressure rise at the balance position.

ARTICLE INFO

Keywords:
Spray
Collapse
Vapor condensation
Flash boiling
Gasoline direct injection engines

ABSTRACT

The main objective of this study is to understand the mechanism of the spray collapse during flash boiling using multi-hole injectors. The spray characteristics of a five-hole gasoline direct injection (GDI) injector were investigated over a range of ambient pressures and fuel temperatures with high-speed imaging and phase Doppler particle measurement techniques. Spray collapses under both flash-boiling and non-flash-boiling (elevated ambient pressure) conditions were observed, but due to different mechanisms. In order to prove that the vapor condensation near the nozzle exit is the primary cause for the collapse under flash boiling conditions, careful analysis to examine the two necessary conditions for vapor condensation in multi-jet flash-boiling sprays was conducted: (1) existence of sub-cooled droplets and (2) existence of saturated vapor. The first condition could be supported by the previous studies and the other condition was numerically and experimentally demonstrated in the present study. It was found that the local static pressure significantly increased at the balance position, where the radial momentums of the droplets and vapor issued from the five holes could be counteracted. The increased static pressure was beyond the local saturation pressure, fulfilling the condition for vapor condensation. Furthermore, the bimodal size distribution under flash boiling conditions and the condensation core inside the spray observed under much reduced ambient pressure also prove the occurrence of vapor condensation at the nozzle exit.

1. Introduction

In recent years, flash boiling has been widely studied due to its great potential in improving spray atomization quality [1–3] and impingement [4] for gasoline direct injection (GDI) engines. A recent report has shown that up to 99% of all the injections during New European Driving Cycle and 95% during 'Real Driving Emissions' tests in mid-range cars were superheated [5]. Therefore, the flash-boiling spray should be fully understood because of its significant impact on atomization and its frequent occurrence in real GDI engines.

Flash-boiling can be achieved by elevating liquid temperature or depressurizing ambient pressure to make the liquid superheated. The superheated degree can be expressed by the temperature difference between the liquid temperature and the saturation temperature at local ambient pressure, or by the ratio of the ambient pressure over the saturation pressure. The superheated fluid inside the nozzle undergoes the processes of nucleation and bubble growth. The mechanisms of nucleation and bubble growth have been investigated and several models have been proposed [6–8]. In order to correlate the inside bubble formation and external superheated jet breakup, a number of studies have been conducted. Zhang et al. [9,10] studied the effect of bubble formation inside a nozzle on the external breakup process of a superheated liquid jet. They found that the bubble number increased with the superheated degree and claimed that bubble number density

* Corresponding author.
E-mail address: chenlongfei@buaa.edu.cn (L. Chen).

https://doi.org/10.1016/j.applthermaleng.2018.01.102
Received 7 May 2017; Received in revised form 18 December 2017; Accepted 27 January 2018
Available online 31 January 2018
1359-4311/

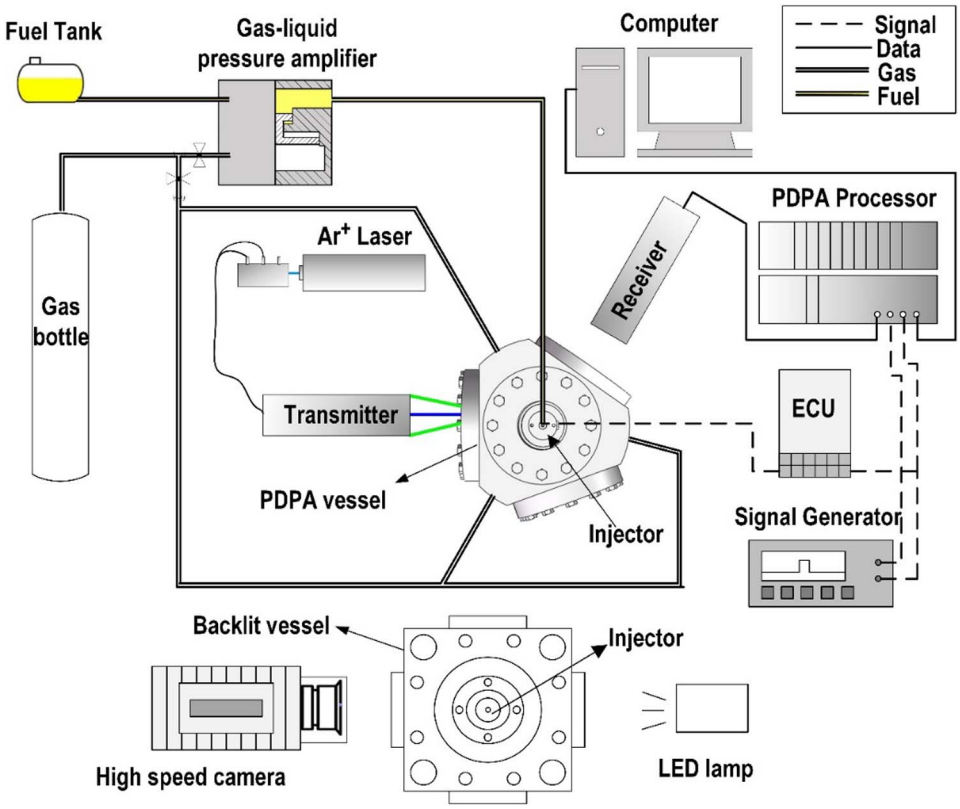

Fig. 1. Schematic of the experiment setup for PDPA and backlit.

could be the main driving force enhancing the superheated liquid jet breakup. With a real-size transparent injector nozzle, Serras-Pereira et al. [3] found that the in-nozzle flow regime was highly sensitive to fuel temperature and the increase in superheated degree dramatically improved primary breakup and atomization. Wang et al. [11] studied the near-field spray characteristics of 2-methylfuran, ethanol and *iso*-octane under flash boiling conditions and reported that saturation ratio and cavitation number were the two dominant factors for the near-nozzle spray behaviors.

It has been widely observed that spray collapse would occur under flash-boiling conditions when multi-hole GDI injectors were used [1–3,12–15]. The occurrence of spray collapse could lengthen spray tip penetration, lead to the fuel film buildup on the cylinder wall and piston crown [16], and increase soot emissions. Furthermore, fuel impingement would also dilute the lubricating oil, which was believed to be one of the sources inducing super-knock [17]. Zhang et al. [12] studied the flow field of the multi-jet flash-boiling sprays and found that the superheated degree was the predominant factor in determining the structure and flow field. Mojtabi et al. [13] studied the effects of fuel properties, superheated degree and nozzle configuration (different envelop cone angles) on the flash-boiling sprays and found that superheated degree and nozzle configuration were the two key parameters affecting spray collapse. Based on experimental results with different liquids and injectors, Kramer et al. [5] suggested that the trajectory deviation could be induced by flash-boiling or increasing nozzle hole number. Yang et al. [14] investigated spray collapse under flash-boiling conditions, and suggested it was attributed to low-pressure zone caused by the high speed jets and the jet overlap. Aori et al. [15] investigated the effect of nozzle configuration on the macroscopic characteristics of flash-boiling sprays, and revealed that the spray collapse was enhanced for nozzles with more holes and symmetrical configuration. They also claimed that the spray collapse was induced by the low-pressure zone enclosed by the high-speed jets.

However, spray collapse could also be observed at elevated ambient pressures (non-flash-boiling conditions) [18–21]. It is worth noting that the spray collapse under non-flash-boiling conditions was also attributable to the generation of low-pressure zone enclosed by high-speed jets [18,20,21], which was used to explain the collapse under flash-boiling conditions as well. Recently, Guo et al. [22] compared the collapse of multi-jet sprays under elevated ambient pressure with the collapse under flash boiling conditions. They found that the spray collapse became much weaker as the ambient pressure decreased from 10.0 bar to 1.0 bar and the spray even slightly expanded as the ambient pressure further decreased to 0.5 bar with the liquid temperature fixed at 20 °C. In other words, the jet-to-jet interaction was very weak at low ambient pressures. This phenomenon can be observed in the current study (Fig. 6). Considering that flash boiling in GDI engines normally occurred at sub-atmospheric pressures, it is unlikely that the collapse under flash boiling conditions was just caused by the jet-to-jet interactions, or to be more precise, the low-pressure zone enclosed and induced by the high-speed jets could not be produced under flash boiling conditions. Thus, Guo et al. [22] further proposed that the spray collapse at elevated ambient pressures was caused by the low pressure zone enclosed and induced by the high-speed jets, while the collapse under flash boiling conditions was caused by the low pressure zone induced by the vapor condensation at the nozzle exit. The two collapse mechanisms with different inner physical process were termed as jet-induced spray collapse and condensation-induced spray collapse, respectively. The proposal of condensation-induced spray collapse was based on a series of findings, which demonstrated that the temperature of the initial superheated liquid immediately dropped below the local saturation temperature at the nozzle exit [23–25]. A recent study from Li et al. [26] reported that the near-field spray width was quite sensitive to P_{amb} under flash boiling conditions. With the increase in superheated degree, relatively larger P_{amb} could enhance the spray collapse while relatively small P_{amb} could enhance the expansion. They suggested that relatively larger P_{amb} be conducive to increasing local vapor concentration via vapor coagulation and enhancing the condensation intensity, leading to stronger collapse, whereas, relatively small P_{amb} may lead to relatively weaker collapse due to the dilute vapor concentration

even though it increases superheated level.

The present research is the continuity of our previous investigation [22,26], and to elaborate the collapse of multi-jet flash-boiling sprays and provide more direct evidence to support the idea that the collapse of multi-jet flash-boiling jets may be caused by the vapor condensation at the nozzle exit. The tests were carried out over a range of ambient pressures and fuel temperatures using a five-hole GDI injector. Spray morphology, droplet velocity and size were captured using high-speed imaging and phase Doppler measurement techniques.

2. Experimental setup

The schematic experimental setup is shown in Fig. 1. Two vessels were used, one for the PDPA measurement and the other for backlit imaging. In the PDPA vessel, two quartz windows were mounted at the side with the intersection angle of 110° in order to achieve the best signal-to-noise ratio for PDPA measurement. The injector was mounted on the top of the vessel and the hole diameter is 0.18 mm. The ambient air flowed constantly through the vessel to purge out the residual droplets. The flow rate was so low that the ambient pressure was kept constant in the vessel. Besides, the influence of airflow on the injection process was negligible. The injection rate was set at 1 Hz, to provide sufficient time for the scavenging. In the backlit vessel, two quartz windows were mounted oppositely. A Photron SA X2 high-speed camera was utilized to visualize the spray morphology, illuminated by an LED light. The camera speed was set as 25,000 fps and the corresponding resolution was 640,768 pixels, with the exposure time of 6.25 μs and the spatial resolution of 0.1 mm/pixel.

A non-axisymmetric five-hole GDI injector with the footprint shown in Fig. 2 was used. Jet **1** was selected as the target jet in PDPA measurement. The injector was mounted in such an orientation that the target jet was perpendicular to the imaging direction and the incident lasers from PDPA. The fuel pressure was realized by a gas-to-liquid pressure amplifier driven by a high-pressure gas bottle.

A set of two-dimensional PDPA system from Dantec was used to measure the droplet diameter and velocity and the relevant parameter settings are shown in Table 1. The laser beam is emitted from an argon-ion laser and it passes through a Bragg cell to be separated into two pairs of laser beams. Then, the laser beams are transferred to the transmitter by optical fibers and focused by the transmitting lens with a focus length of 310 mm. The focus point determines the measurement volume of PDPA. When the droplet travels through the measurement volume, the scattered signal could be captured by the receiver and be subsequently processed by the PDPA processer to obtain the droplet diameter and velocity values.

The measurement positions are shown in Fig. 3. The injector axis and the nominal axis of the target jet have been marked by dashed lines, respectively. The axial distance from the measurement points to the injector tip ranged from 15 to 30 mm. In the radial direction, the measurement points spread from the spray edge to the injector axis with the interval of 1 mm. The measurement lasted 60 s in each position with the maximum sample count of 50,000.

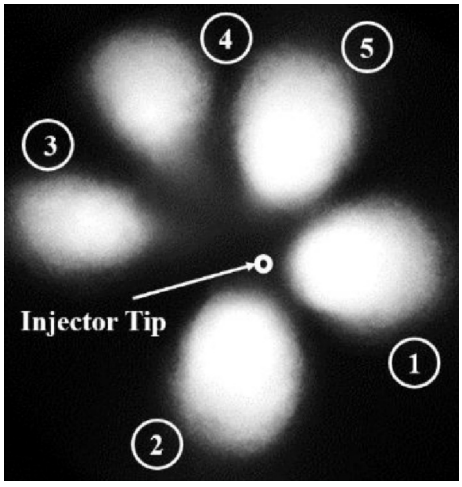

Fig. 2. Spray footprint.

Table 1
Parameter settings for PDPA.

Parameters	Value
Laser power (Watt)	0.8
Wave length (nm)	514.5 & 488.0
Focal length (mm)	310
Receiver type	112 Fiber PDA
Scattering angle (°)	70

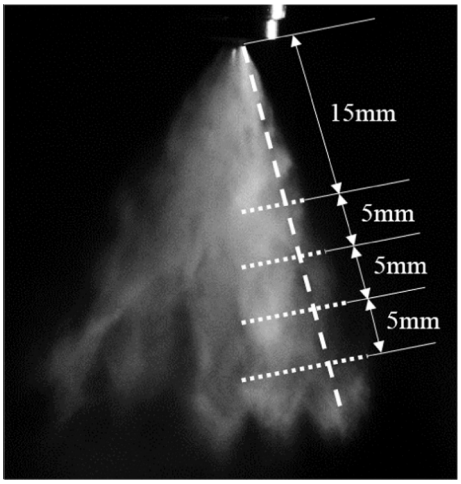

Fig. 3. PDPA measurement positions.

The test conditions are listed in Table 2. The ambient pressure ranged from 0.2 bar to 10.0 bar. The fuel temperatures were from 20 °C and 120 °C. For PDPA tests, the liquid temperature ranged from 20 °C and 80 °C and was controlled by the water jacket around the injector. For backlit tests, the liquid temperature was controlled by the heating elements inserted into the injector adaptor. The injection pressure was fixed at 10.0 MPa and the injection duration was 1.5 ms. A mainstream gasoline with the RON (research octane number) of 95 was used as the injection liquid and the distillation curve is shown in Fig. 4.

The image processing procedure to extract spray width using in-house MATLAB codes is given in Fig. 5. Fig. 5(a) presents a typical spray image. By background subtraction and image contrast enhancement (Fig. 5(b)), the intensified image was binarized with the threshold values based on Ostu's method, as shown in Fig. 5 (c). Because the background is similar, the variation of threshold values for different conditions is less than 2.6%. In Fig. 5(d), the edge of the spray was obtained from the binarized image. Finally, the spray width was obtained by measuring the distance from the injector axis to the right side of the spray because the right jet was the target jet. The tests were repeated 5 times for each test condition and the averaged spray widths

Table 2
Experiment conditions.

Ambient pressure/bar	0.2, 0.5, 0.8, 1.0, 5.0, 10.0
Fuel temperature/°C	20, 40, 60, 80, 100, 120
Injection pressure/MPa	10.0
Injection duration/ms	1.5
Fuel	Gasoline

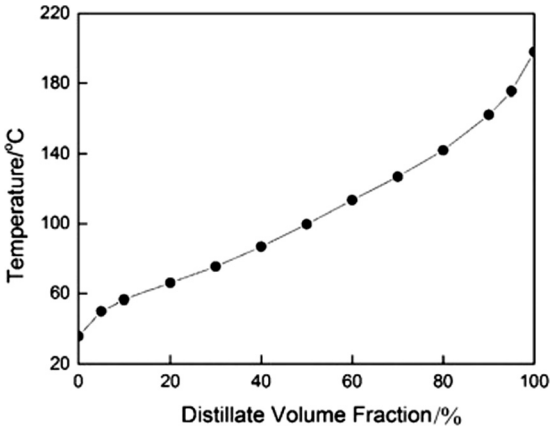

Fig. 4. Distillation curve of test gasoline fuel.

were used.

3. Results

3.1. Spray morphology at different P_{amb}

Fig. 6(a)–(f) presents the spray images under different ambient pressures, at 1.6 ms after the start of trigger (ASOT) when the spray was fully developed. To quantitatively investigate the spray morphology, the evolution of spray width along the injector axis is plotted in Fig. 6(g). Clearly, with the increase in ambient pressure, the spray penetration length becomes shorter due to the increased drag force. In addition, the ambient pressure plays an important role in the spray radial dispersion. The spray width becomes narrower as the ambient pressure varies from 0.2 bar to 1.0 bar, as shown in Fig. 6(g). As the ambient pressure further increases to 5.0 bar and 10.0 bar, the spray widths have more prominent reduction in the near field, indicating the obvious spray collapse at the elevated ambient pressures. In the far field (after the transition points, as marked in Fig. 6(g)), the spray widths at elevated ambient pressures significantly increase. Furthermore, with the increase in ambient pressure from 5.0 bar to 10.0 bar, the transition length decreases from 5.46 mm to 4.78 mm. The collapse occurring at elevated ambient pressures of 5.0 and 10.0 bar can be attributed to the strong jet-to-jet interaction and the resultant low-pressure zone enclosed by the jets [18]. The failure to observe the similar phenomenon at the ambient pressures less than 5.0 bar is owing to weakened jet-air interaction.

The far-field increase in spray width along with the axis can be explained by the numerical study from Khan et al. [27]. It was caused by the collision between the downward gas due to the entrainment near the nozzle exit and the upward gas flow from the far field. The collision led to a stagnation plane in the vertical direction and forced the gas to expand radially, as well as the droplets. As the ambient pressure increases, the decreased jet velocity could cause the stagnation plane to move upward, i.e. the transition length decreased as the ambient pressure increased from 5.0 bar to 10.0 bar in the present study.

3.2. Spray morphology at different T_{fuel}

Fig. 7 gives the images with different fuel temperatures and the evolution of spray width along the injector axis. The ambient pressure is fixed at 0.5 bar. With the increase in fuel temperature, the gap between the jets diminishes, and the jets merges into one jet after the temperature of 80 °C. As shown in Fig. 7(g), the near-field spray widths for the fuel temperatures of 20, 40, 60 and 80 °C are almost identical and increases as the fuel temperature increases to 100 and 120 °C due to the enhanced bubble bursting. At the axial distance larger than 7.5 mm, the spray width decreases with the increase of fuel temperature, indicating the collapse of the spray. Therefore, during flash boiling, the spray undergoes an expansion and then collapse process, showing the reverse trend in Fig. 6.

3.3. Droplet motions

Fig. 8 presents the effect of ambient pressure on the droplet velocity distribution at the fuel temperatures of 20 °C and 80 °C at the timing of 1.6 ms ASOT. At the cases of 20 °C (top row), the peak droplet velocity in each axial position generally near the jet axis at the ambient pressures of 0.5 and 1.0 bar, indicating the absence or negligible existence of spray deflection. However, large difference can be observed at the ambient pressure of 10.0 bar. At the axial distance of 15 mm, few droplets are present at the outer side of the target jet and the droplet velocity in the inner side moves towards to the injector axis, rather than along with the jet axis. At the axial distance of 20 mm, the droplets moves towards the outer side. The droplet movements at 15 and 20 mm match very well with spray collapse and radial expansion, as shown in Fig. 6.

As the fuel temperature increases to 80 °C (bottom row), the droplet velocity distribution at the ambient pressure of 0.5 bar is significantly different. The droplets generally moves to downstream vertically, rather than along the spray axis, as shown in Fig. 8(d). Slight deflection is observed at the ambient pressure of 1.0 bar as the peak velocity at each axial distance obviously occurs at the inner side of the jet axis, as shown in (Fig. 8(e)). This slightly enhanced deflection in contrast to the case of 20 °C (Fig. 8(b)) may be attributed to the slight flash boiling of the light components of gasoline and reduced liquid viscosity due to the increased fuel temperature. At the ambient pressure of 10.0 bar, the peak velocity at the axial distance of 15 mm occurs at the third position from the left in the case of fuel temperature of 20 °C (Fig. 8(c)) while the peak velocity appears at the first position from the left in the same axial distance, seen in Fig. 8(f). The enhanced deflection at elevated fuel

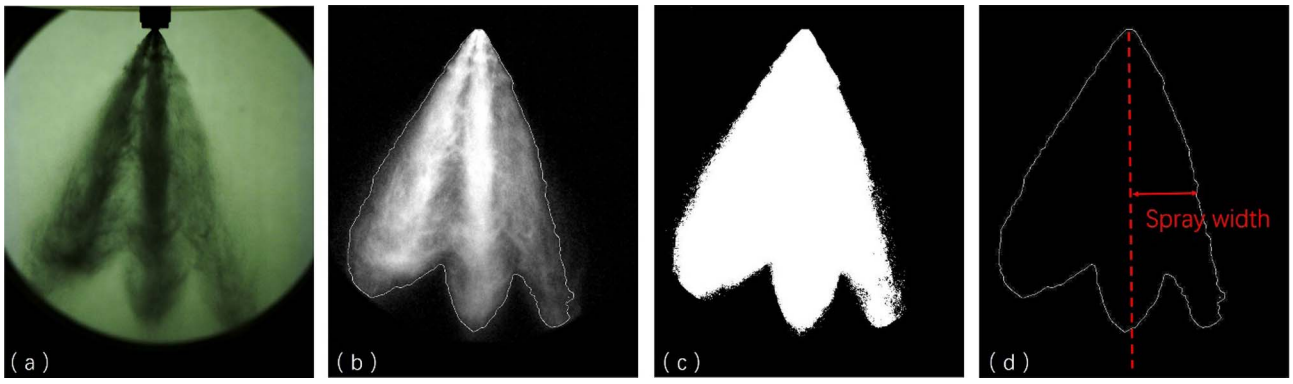

Fig. 5. Illustrative procedure of image processing.

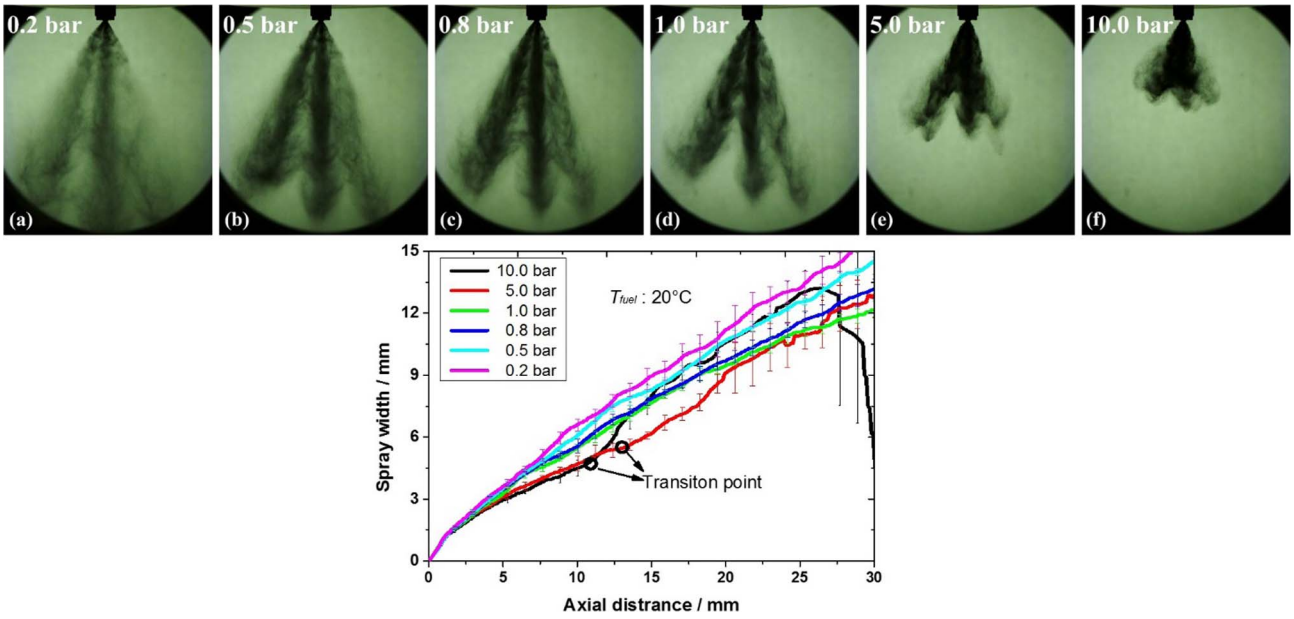

Fig. 6. Spray images and widths at ambient pressures from 0.2 bar to 10.0 bar (T_{fuel} = 20 °C, 1.6 ms ASOT).

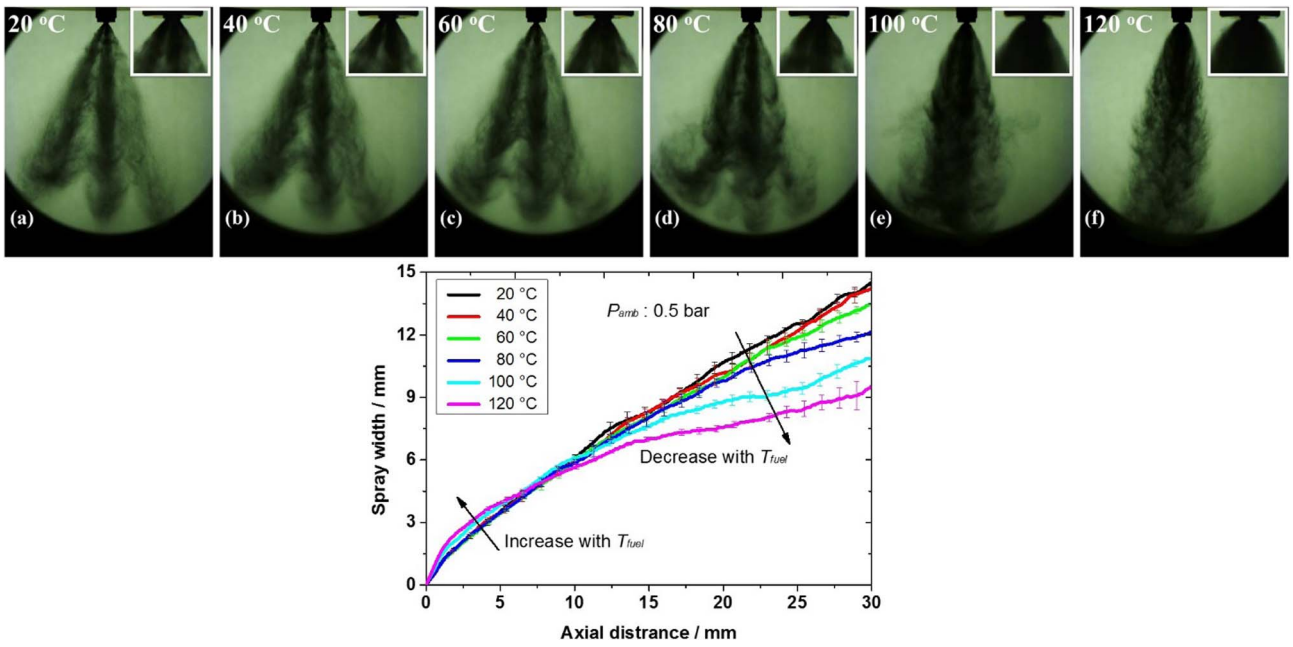

Fig. 7. Spray images and widths at fuel temperatures from 20 °C to 120 °C (P_{amb} = 0.5 bar, 1.6 ms ASOT).

temperature in the cases of 1.0 and 10.0 bar is attributed to the increased exit velocity and pressure difference, which were caused by the reduced viscosity and liquid density as the fuel temperature increases.

4. Discussion

The collapse under elevated ambient pressures and flash boiling conditions shown Figs. 6 and 7 could be attributed to the jet-induced low pressure zone and the vapor condensation-induced low pressure zone, respectively [18]. With regard to the proposed condensation-induced low-pressure zone, it can well explain the collapse under flash boiling conditions, but stronger evidences are needed to support the occurrence of vapor condensation and this is the original objective of the present study.

Two conditions have to be fulfilled for occurrence of vapor condensation: (1) existence of sub-cooled droplets as the nuclei; and (2) the vapor partial pressure of injected substance much be higher than the local saturation pressure. Considering that GDI sprays are highly transient (e.g. injection duration of 1.5 ms in the present study) and vapor condensation occurs in the dense area, it is quite difficult to directly observe this process. Thus, the main efforts in the following Sections 4.1 and 4.2 are to demonstrate the fulfillment of the two necessary conditions abovementioned based on the available findings and a simplified simulation, respectively. Then, in Sections 4.3 and 4.4, further analysis on the droplet size distribution and the inner structure of flashing spray was examined to support the existence of vapor condensation phenomenologically.

4.1. Existence of sub-cooled droplets

For flash boiling sprays, it has been widely reported that the liquid temperature at the nozzle exit dropped to the ones below the local

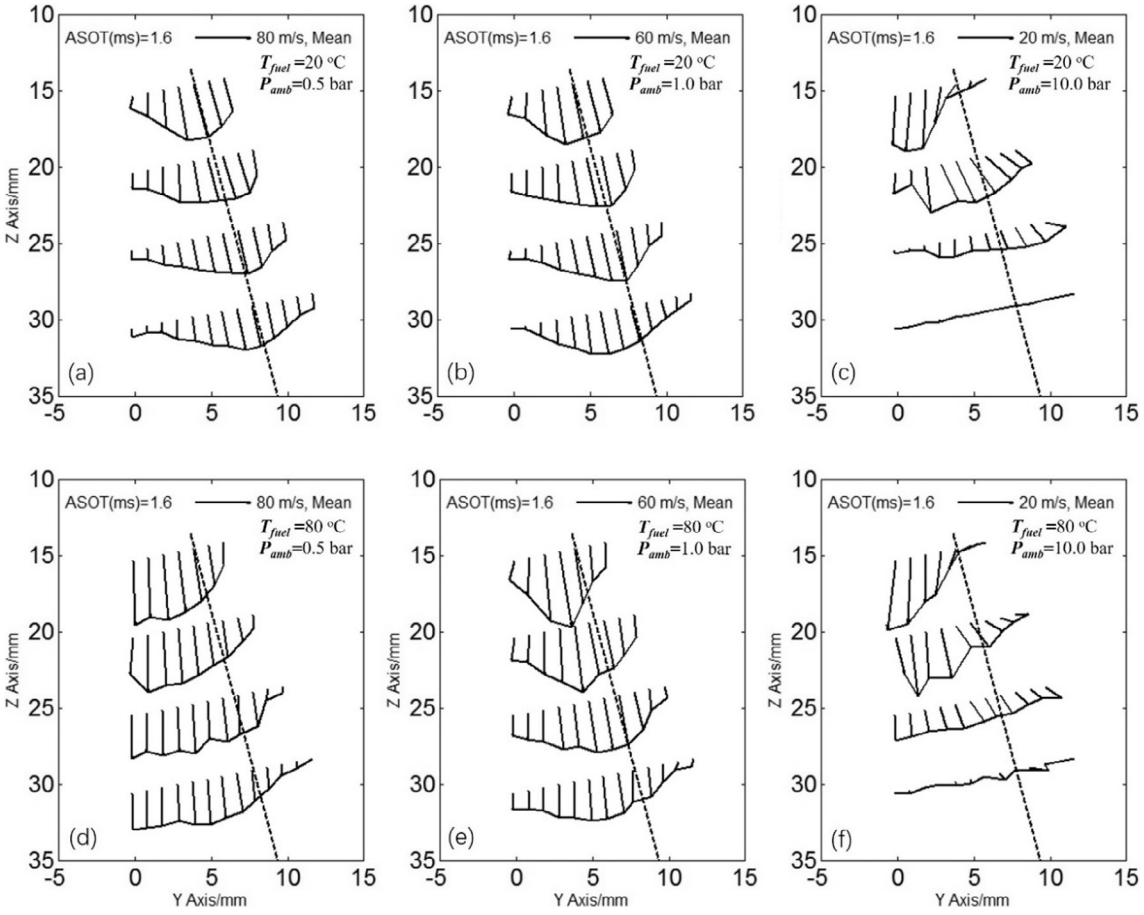

Fig. 8. Droplet velocity distributions at different conditions (Timing: 1.6 ms ASOT).

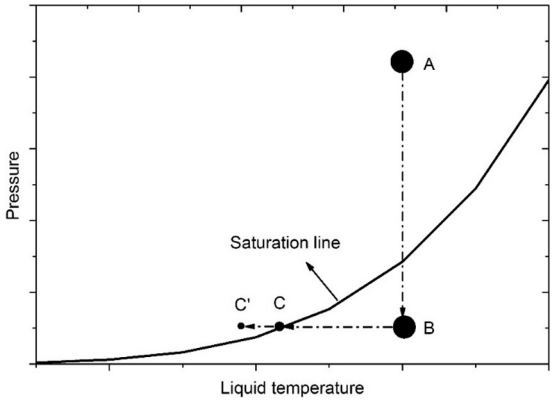

Fig. 9. Schematic of liquid temperature evolution from high-pressure to depressurized condition.

saturation temperature. This phenomenon not only occurs for the substances which are liquid in the standard condition, e.g. water [24], but also for those which are gaseous in the standard condition, e.g. liquid R134a [23], liquid CO_2 [28] and liquid N_2 [25]. The solid state of CO_2 and N_2 was observed during the superheated liquid spray [25,28]. Fig. 9 schematically describes the liquid temperature evolution during superheated sprays. Once the heated liquid (state *A*) is suddenly injected to environment with ambient pressure less than its saturation pressure, it will become superheated (state *B*). To achieve the thermodynamic equilibrium (*C* or beyond *C*), violent evaporation and breakup would occur to release contained energy. According to above discussion [23–25,28], the temperature of the residual liquid would be less than its saturation temperature (e.g. ***C′***), rather than that at ***C*** at the end of flash boiling. In other words, the residual liquid becomes subcooled for a given ambient pressure.

4.2. Existence of saturated vapor

In addition, the vapor phase should have a lower temperature than $T_{C'}$ due to the bubble bursting and could condense once the partial pressure is larger than $P_{sat}(T_{C'})$, which is lower than the ambient pressure, $P_{sat}(T_C)$. Considering that the initial ambient gas below the injector should be pushed away once the spray starts, the gas phase inside the spray and near the nozzle exit is mainly composed of the fuel vapor. Thus, the partial pressure is the ambient pressure, which is larger than $P_{sat}(T_{C'})$. Thus, the existence of saturated vapor is established.

Besides, jet overlap is another important process to produce saturated vapor. Fig. 10 schematically gives the jet expansion process. Once the needle starts to move upwards, a number of bubbles form as the superheated fuel flows through the nozzle. Consequently, dramatic radial expansion would occur as the fuel leaves the nozzle due to the bubble bursting, as shown in Fig. 10(b). With the continuous expansion, jet overlap would occur, as shown in Fig. 10(c). Different from flash-boiling sprays using single-hole injectors, which is freely dispersed, a balance position can be formulated for the present multi-hole GDI injectors and the radial momentums of droplets from the five jets can be counteracted, leading to the dramatic increase in static local pressure. This local pressure increase is thought to produce the saturated vapor.

In order to deliver a semi-quantitative analysis on the static pressure distribution from the hole exit to the balance position, a simplified model to simulate the pressure increase is established. The target area is the red rectangle marked in Fig. 10(c). The simplified geometrical model is shown in Fig. 11(a). The gas flow from the left side (hole exit)

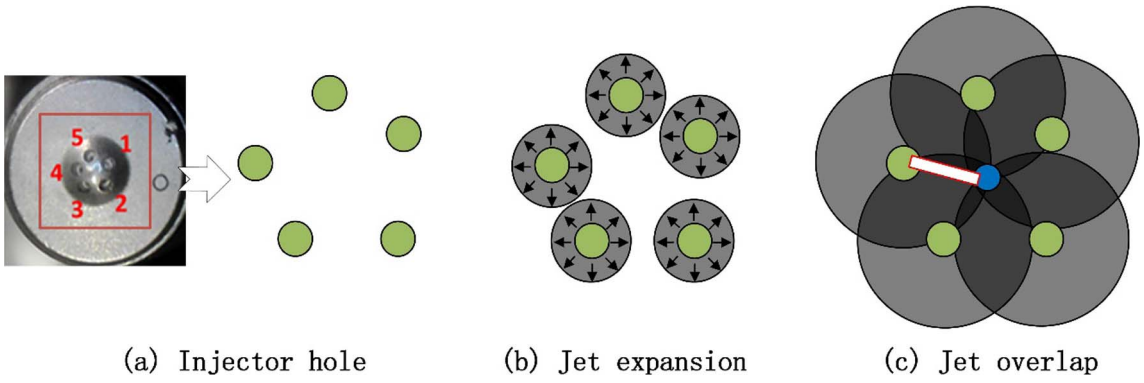

Fig. 10. Illustration of the jet overlap.

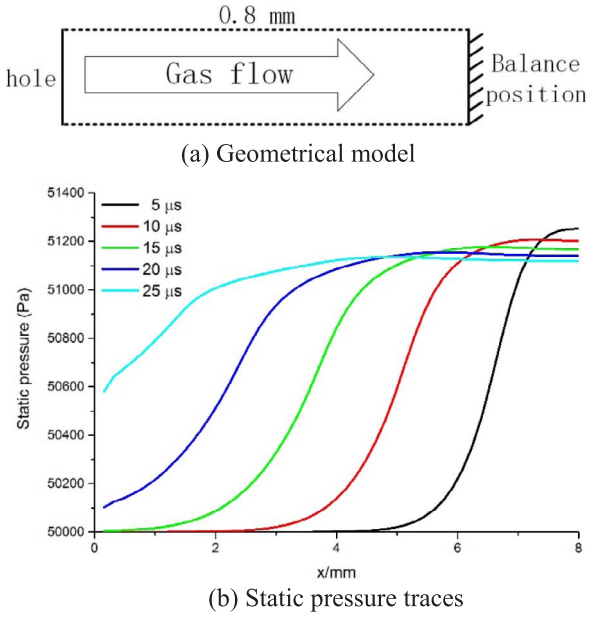

Fig. 11. Geometrical model and static pressure traces.

moves towards to the closed end (balance position) with a speed of 20 m/s. The distance is 0.8 mm and the initial ambient pressure is 50 kPa. Fig. 11(b) gives the pressure traces with the time from 5 μs to 25 μs with a time step of 5 μs. Clearly, at the closed end, the pressure value is higher than the ambient pressure by 1200 Pa instantly.

Back to the multi-jet overlap process, it is easy to understand that a locally larger static pressure would occur and exceed the local saturation pressure immediately. One assumption is made that the vast majority of the substance near the nozzle exit is the injected fuel, including liquid and vapor phase. This assumption is reasonable because the strong expansion caused by the vapor bursting would push away the ambient gas below the injector tip and gas entrainment can only start at certain distances from the nozzle tip [29]. Thus, the other necessary condition for condensation that there is saturated vapor pressure now is also established.

4.3. Droplet size distribution

Fig. 12 presents the droplet size distribution for the position at the distance of 20 mm vertically below the injector tip. The given ambient pressures are 0.5, 1.0 and 10.0 bar with the fuel temperature fixed at 80 °C. Clearly, a typical unimodal distribution is observed under the ambient pressure of 10.0 bar. For the size distribution at the ambient pressure of 1.0 bar, there is a sudden increase in the droplet percentage between 1.5 μm and 3.0 μm and it may be attributed to the low-pressure

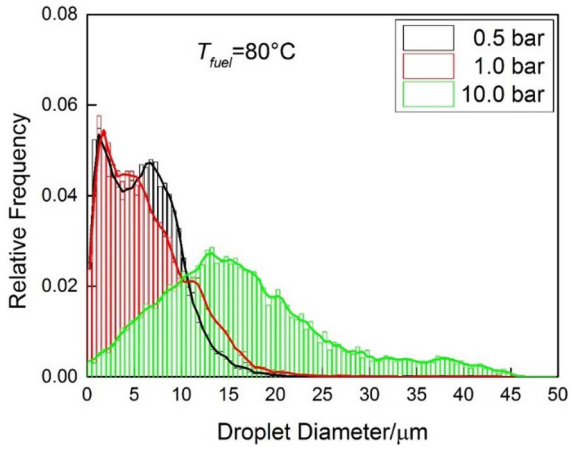

Fig. 12. Droplet size distribution at different ambient pressures.

zone, which could suck small droplets in the zone [21]. Interestingly, the distribution under the ambient pressure of 0.5 bar, where flash boiling occurs, bimodal distribution was found. Similar bimodal size distributions were also found in previous studies under flash boiling conditions [30,31] and it was attributed to the vapor condensation. The explosive bubble bursting could produce a plenty of small droplets. The small droplets are more inclined to be the condensation nuclei and produce one more peak in the distribution because they have much more rapid temperature drop than that of large droplets. However, further investigation is needed to confirm that.

4.4. Liquid core under extremely low ambient pressures

An additional group of proof tests was carried out in the same test bench with the liquid temperature fixed at 120 °C but much reduced ambient pressures. The spray images at 1.6 ms ASOT are provided in Fig. 13 and the ambient pressures are 0.1, 0.05 and 0.02 bar. Clearly, the spray width increased significantly with the decrease in ambient pressure. The greatly increased spray width can be attributed to the following two factors: (1) the decrease in ambient pressure reduces the resistance of radial expansion of the spray; (2) the decrease in ambient pressure also increases the superheated degree, and this could enhance the generation of bubbles and the intensity of bubble bursting.

The significant expansion with the reduced ambient pressure causes the spray field to be more dilute, making it possible to identify the inner structure of the flash-boiling spray. The images under the ambient pressures of 0.05 and 0.02 bar are partially enhanced in order to present the inner structure. Clearly, a blob is found near the injector tip, followed by a strip-like dark area can be observed. Comparing the enhanced image in Fig. 13(b) with Fig. 7(f), as shown in Fig. 14, the projected angles between the spray axis and the injector axis in

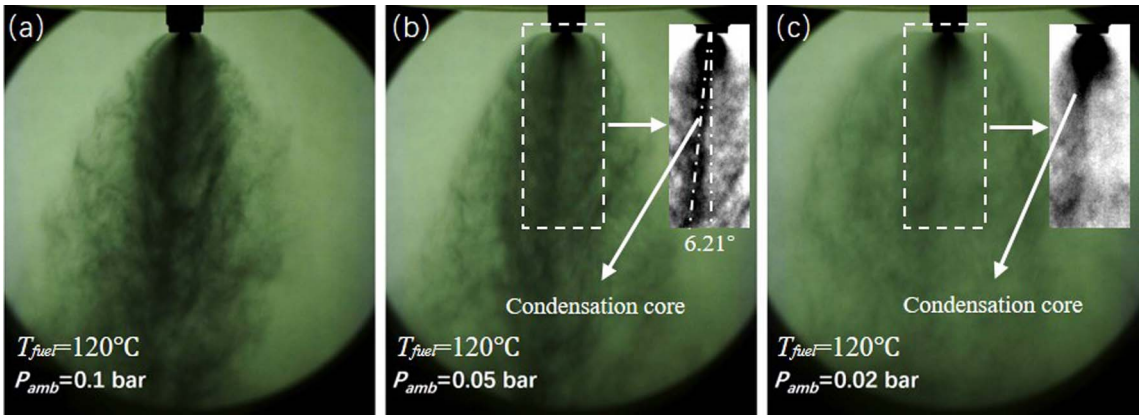

Fig. 13. Spray images at much reduced ambient pressures.

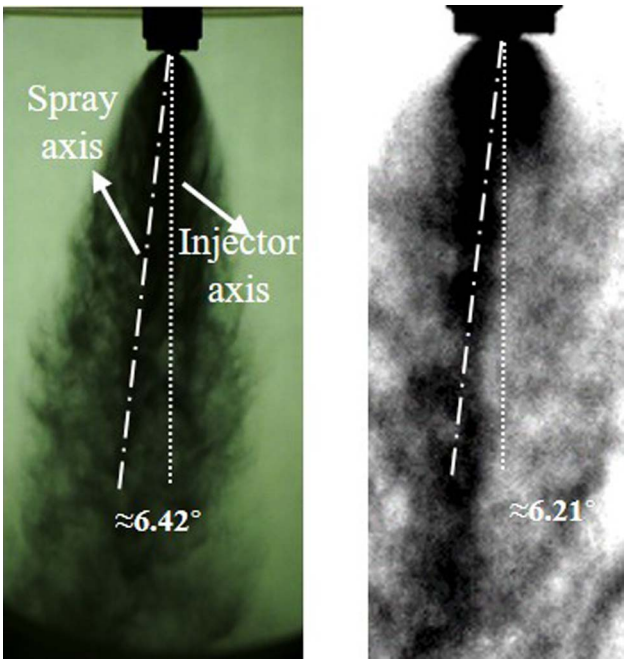

Fig. 14. Angles of the spray axis and the injector axis (T_{fuel}: 120 °C; P_{amb}: 0.5 bar (Left), 0.05 bar (Right)).

Fig. 14(a) is almost equal to the projected angle between the strip-like dark area and the injector axis in Fig. 14(b). The strip-like dark area is believed to be the condensation core.

5. Conclusions

The present research examined the spray morphology over a wide range of fuel temperatures and ambient pressures, and demonstrated that the collapse of multi-jet flash-boiling sprays was induced by vapor condensation at the nozzle exit. Main conclusions can be drawn as follows:

(1) The collapse of multi-jet flash-boiling sprays was attributed to the vapor condensation, which was caused by liquid temperature plunge and the local static pressure increase due to the counteraction of the radial momentums of droplets and vapor from different jets;
(2) Bimodal size distribution under flash boiling conditions was observed and the appearance of the peak at smaller diameter was considered to be caused by vapor condensation;
(3) The significantly reduced ambient pressure provided a chance to observe the inner structure of collapsed multi-jet flash-boiling sprays, which were mainly composed of a blob near the nozzle exit and a following strip-like dense area.

It is worth noting that nozzle configuration also plays an important role in determining whether the spray collapses or not. More quantitative data should be provided using advanced CFD tools and by the implementation of advanced diagnostic techniques. The physical reasons for the existence of sub-cooled droplets at local ambient pressure also need more in-depth investigation.

Acknowledgement

This work was supported by National Natural Science Foundation of China under the Grant of 51406103.

References

[1] H. Guo, X. Ma, Y. Li, S. Liang, Z. Wang, H. Xu, J. Wang, Effect of flash boiling on microscopic and macroscopic spray characteristics in optical gdi engine, Fuel 190 (2017) 79–89.
[2] Z. Wang, X. Ma, Y. Jiang, Y. Li, H. Xu, Influence of deposit on spray behaviour under flash boiling condition with the application of closely coupled split injection strategy, Fuel 190 (2017) 67–78.
[3] J. Serras-Pereira, Z. van Romunde, P.G. Aleiferis, D. Richardson, S. Wallace, R.F. Cracknell, Cavitation, primary break-up and flash boiling of gasoline, iso-octane and n-pentane with a real-size optical direct-injection nozzle, Fuel 89 (2010) 2592–2607.
[4] Z. Wang, Y. Li, H. Guo, C. Wang, H. Xu, Microscopic and macroscopic characterization of spray impingement under flash boiling conditions with the application of split injection strategy, Fuel 212 (2018) 315–325.
[5] M. Kramer, E. Kull, M. Wensing, Flashboiling-induced targeting changes in gasoline direct injection sprays, Int. J. Engine Res. 17 (2016) 97–107.
[6] M. Plesset, S.A. Zwick, The growth of vapor bubbles in superheated liquids, J. Appl. Phys. 25 (1954) 493–500.
[7] D.W. Oxtoby, Homogeneous nucleation: theory and experiment, J. Phys.: Condens. Matter 4 (1992) 7627.
[8] E. Sher, T. Bar-Kohany, A. Rashkovan, Flash-boiling atomization, Prog. Energy Combust. Sci. 34 (2008) 417–439.
[9] S. Li, Y. Zhang, B. Xu, Correlation analysis of superheated liquid jet breakup to bubble formation in a transparent slit nozzle, Exp. Therm Fluid Sci. 68 (2015) 452–458.
[10] Y. Zhang, S. Li, B. Zheng, J. Wu, B. Xu, Quantitative observation on breakup of superheated liquid jet using transparent slit nozzle, Exp. Therm Fluid Sci. 63 (2015) 84–90.
[11] B. Wang, C. Wang, X. Bao, Y. Li, H. Xu, Microscopic investigation of near-field spray characteristics of 2-methylfuran, ethanol and isooctane under flash boiling conditions, Fuel (2018).
[12] M. Zhang, M. Xu, Y. Zhang, G. Zhang, D.J. Cleary, Flow-field investigation of multi-hole superheated sprays using high-speed piv. Part I. Cross-sectional direction 22 (2012) 983-995.
[13] M. Mojtabi, G. Wigley, J. Helie, The effect o flash boilig on the atomizatio performance of gasoline direct injection multistream injectors, Atomiz. Sprays 24 (2014) 467–493.
[14] S. Yang, Z. Song, T. Wang, Z. Yao, An experiment study on phenomenon and mechanism of flash boiling spray from a multi-hole gasoline direct injector, Atomiz. Sprays 23 (2013) 379–399.

[15] G. Aori, D.L.S. Hung, M. Zhang, G. Zhang, T. Li, Effect of nozzle configuration on macroscopic spray characteristics of multi-hole fuel injectors under superheated conditions, Atomiz. Sprays 26 (2016) 439–462.
[16] Z. Wang, H. Guo, C. Wang, H. Xu, Y. Li, Microscopic level study on the spray impingement process and characteristics, Appl. Energy 197 (2017) 114–123.
[17] Z. Wang, H. Liu, R.D. Reitz, Knocking combustion in spark-ignition engines, Prog. Energy Combust. Sci. 61 (2017) 78–112.
[18] Y. Li, H. Guo, X. Ma, J. Wang, H. Xu, Droplet dynamics of di spray from sub-atmospheric to elevated ambient pressure, Fuel 179 (2016) 25–35.
[19] R. Payri, F.J. Salvador, P. Martí-Aldaraví, D. Vaquerizo, Ecn spray g external spray visualization and spray collapse description through penetration and morphology analysis, Appl. Therm. Eng. 112 (2017) 304–316.
[20] K. Nishida, J. Tian, Y. Sumoto, W. Long, K. Sato, M. Yamakawa, An experimental and numerical study on sprays injected from two-hole nozzles for disi engines, Fuel 88 (2009) 1634–1642.
[21] S. Malaguti, S. Fontanesi, G. Cantore, Numerical characterization of a new high-pressure multi-hole gdi injector, in: ILASS Europe, 2010.
[22] H. Guo, H. Ding, Y. Li, X. Ma, Z. Wang, H. Xu, J. Wang, Comparison of spray collapses at elevated ambient pressure and flash boiling conditions using multi-hole gasoline direct injector, Fuel 199 (2017) 125–134.
[23] Z. Zhou, W. Wu, B. Chen, G. Wamg, L. Guo, An experimental study on the spray and thermal characteristics of r134a two-phase flashing spray, Int. J. Heat Mass Transf. 55 (2012) 4460–4468.
[24] A. Günther, K.E. Wirth, A. Bräuer, P. Siegler, B. Köninger, Temperature characteristics in a flash atomization process, Atomiz. Sprays 26 (2016) 1337–1359.
[25] M. Luo, O.J. Haidn, Characterization of flashing phenomena with cryogenic fluid under vacuum conditions, J. Propul. Power 32 (2016) 1253–1263.
[26] Y. Li, H. Guo, X. Ma, Y. Qi, Z. Wang, H. Xu, S. Shuai, Morphology analysis on multi-jet flash-boiling sprays under wide ambient pressures, Fuel 211 (2018) 38–47.
[27] M. Khan, J. Helie, M. Gorokhovski, A. Wood, G. Wigley, J. Kashdan, J. Dumas, M. Mojtabi, P. Guibert, Numerical analysis of multihole gasoline direct injection sprays, in: 12th International Conference on Liquid Atomization and Spray Systems, Heidelberg, Germany, 2012.
[28] T.-C. Lin, Y.-J. Shen, M.-R. Wang, Effects of superheat on characteristics of flashing spray and snow particles produced by expanding liquid carbon dioxide, J. Aerosol Sci. 61 (2013) 27–35.
[29] R.K. Calay, A.E. Holdo, Modelling the dispersion of flashing jets using cfd, J. Hazard. Mater. 154 (2008) 1198–1209.
[30] L.A. Dombrovskii, V.I. Zalkind, Y.A. Zeigarnik, D.V. Marinichev, V.L. Nizovskii, A.A. Oksman, K.A. Khodakov, Atomization of superheated water: results from experimental studies, Therm. Eng. 56 (2009) 191–200.
[31] K. Breton, B.A. Fleck, D. Nobes, A parametric study of a flash atomized water jet using a phase doppler particle analyzer, Atomiz. Sprays 23 (2013) 799–817.